Energy Storage Materials 10 (2018) 206–215

Contents lists available at ScienceDirect

Energy Storage Materials

journal homepage: www.elsevier.com/locate/ensm

Lightweight, free-standing 3D interconnected carbon nanotube foam as a flexible sulfur host for high performance lithium-sulfur battery cathodes

Raghunandan Ummethala[a], Martin Fritzsche[a], Tony Jaumann[a], Juan Balach[a,b], Steffen Oswald[a], Rafał Nowak[c], Natalia Sobczak[c], Ivan Kaban[a], Mark H. Rümmeli[a,d,e], Lars Giebeler[a,*]

[a] Leibniz Institute for Solid State and Materials Research (IFW) Dresden e.V., Institute for Complex Materials, Helmholtzstr. 20, D-01069 Dresden, Germany
[b] Department of Chemistry, Universidad Nacional de Río Cuarto-CONICET, Route 36 km 601, AR-X5804ZAB Río Cuarto, Argentina
[c] Foundry Research Institute, Center for High-Temperature Studies, ul. Zakopiańska 73, PL-30-418 Cracow, Poland
[d] College of Physics, Optoelectronics and Energy & Collaborative Innovation Center of Suzhou Nano Science and Technology, Soochow University, CN-215006 Suzhou, China
[e] Centre of Polymer and Carbon Materials, Polish Academy of Sciences, ul. M. Curie-Skłodowskiej 34, PL-41-819 Zabrze, Poland

ARTICLE INFO

Keywords:
Lithium-sulfur battery
Carbon nanotube foam
Composite cathode
Free-standing electrode
High sulfur loading

ABSTRACT

The still hindered practical application of lithium-sulfur (Li-S) batteries with a high theoretical energy density of 2.6 kWh kg^{-1} can only be feasible by a simple and scaling-up fabrication of highly stable sulfur-based cathodes. Herein, a free-standing, mechanically flexible, binder-free 3D interconnected carbon nanotube 'foam' (CNTF) is prepared by a single-step facile method and used as a sulfur host in Li-S batteries. For the first time, such a simple method has been adopted for the preparation of free-standing CNT scaffolds for use in Li-S cells, as our method is free from the widely reported solvent-based techniques such as vacuum infiltration of CNTs to obtain free-standing forms but requires further purification and/or drying. A high-areal sulfur loading of 7.1 mg_S cm^{-2}, accounting to a total electrode mass of 10.9 $mg_{electrode}$ cm^{-2}, with yet high electrochemical sulfur utilization of 72% is achievable by the foam-like CNT structure. Reversible areal capacities of up to 9 mAh cm^{-2} at extremely low electrode weight (800 mAh $g_{electrode}^{-1}$) and specific capacities up to 1378 mAh g_S^{-1} are demonstrated. The interconnected porous network acts as a reservoir for trapping soluble lithium polysulfide compounds and greatly improves the sulfur reutilization. The lightweight CNT scaffold further provides enduring electrical contact with the sulfur species, resulting in excellent cycling stability and a potentially high gravimetric energy density desirable for automobiles and aerospace applications. The CNTF/sulfur composite cathode exhibits better rate performance and cycling stability than most of the recently reported CNT-based cathode materials for Li-S batteries.

1. Introduction

Advanced battery systems are in ever-increasing demand in portable electronic devices to huge electric vehicles. The limitations of battery systems in terms of energy density or power density are constantly being challenged over the last few decades. The need for high performance, rechargeable batteries has been on the rise mainly owing to their potential use in transportation-electrical vehicles, aerospace applications and smart grid applications. In this context, Li-S batteries stand out for their high discharge capacities. Sulfur as a cathode material offers unique advantages such as a high theoretical specific capacity (1672 mAh g^{-1}) and its high abundance making it a cost-effective choice [1–3]. However, practical Li-S batteries exhibit considerable capacity fading during the discharging-charging cycles due to a continuous loss of active material in each successive cycle. The intermediate high-order polysulfide compounds (Li_2S_x; $8 \geq x \geq 4$) that form during the discharge reactions tend to dissolve in the surrounding electrolyte, causing a decline in the available active material for subsequent cycles. Furthermore, the high-order polysulfides penetrate through the separator and deposit onto the Li anode to be reduced to insoluble low-order polysulfides, Li_2S/Li_2S_2. While the high-order polysulfides diffuse back and forth in this manner, the low order polysulfides deposit on the anode surface and reduce the active surface area. This undesired process, referred to as polysulfide shuttle mechanism, leads to parasitic self-discharge and low Coulombic efficiency [4–8].

Many efforts have been made to address the aforementioned problems, often by (i) developing novel carbon nanostructured scaffolds that facilitate higher mass loading of sulfur and accommodate high volumetric expansion [9–17], (ii) formulating new electrolytes

* Corresponding author.
E-mail address: l.giebeler@ifw-dresden.de (L. Giebeler).

http://dx.doi.org/10.1016/j.ensm.2017.04.004
Received 13 January 2017; Received in revised form 17 March 2017; Accepted 18 April 2017
Available online 25 May 2017

with reduced solubility of polysulfide compounds [18,19] and (iii) designing porous carbon coated separators/interlayers to inhibit the polysulfide shuttle process [20–22]. Insertion of an interlayer or a mesoporous carbon-coated separator helps in retaining the dissolved polysulfide compounds at the cathode site during cycling. Balach et al. performed direct modification of a commercial polypropylene separator allowing the integration of a conductive mesoporous carbon layer, which acts as a physical medium to localize dissolved polysulfide intermediates and retain them as active material on the cathodic side to improve its reutilization [21]. Alternatively, versatile carbon nanotube (CNT)/graphene-based cathodes are gaining importance due to their light weight, good electrical conductivity and ability to trap polysulfide species, also accommodating volumetric expansion due to their adequate pore volume. Traditionally, CNTs are mixed with elemental sulfur powder, with or without a binder, and are wet ball-milled to obtain a homogenous slurry which is then coated on an aluminum foil or dried and pressed on metallic foam collectors [23,24]. In a bid to further reduce the inactive mass (i.e. binder and current collector) of the electrode, free-standing CNT-based electrodes are being developed. Diverse methods of CNT synthesis and post-treatments are reported. Most of the procedures commonly involve preparation of a liquid dispersion containing elemental sulfur powder and CNTs as the first step. The solution is then ultrasonicated and vacuum filtered in order to obtain a CNT-sulfur composite paper electrode that is further washed and dried to remove the solvent before use. This procedure has proven to be universally applicable for most variants of carbon nanostructures including CNTs, carbon nanofibers and graphene, where in some cases the electrode offers mechanical flexibility as well [11,13,15,16,25]. However, the ratio of carbon and sulfur needs to be carefully controlled in order to maintain the electrical conductivity and physical shape of the electrode. On the down side, the use of solvent-based methods with isolating binders deteriorate the outstanding electronic properties of the CNTs and the preparation methods are often cumbersome, involving several steps followed to ensure a homogenous distribution of sulfur and removal of the solvent eventually. Furthermore, the procedure may not remain facile, cost-effective or environmentally-friendly when scaled up to commercial production. Literature concerning easy-to-perform and resource-preserving procedures to prepare free-standing, binder-free, flexible sulfur-containing electrodes is hitherto very limited [26,27]. Although some of the most recent reports suggested innovative ways to entrap polysulfide species within the electrode and enhance the electrochemical performance, (a) their synthesis methods are far more complicated than our technique and (b) their electrochemical performance at high mass loading of sulfur is much poorer in their studies leading to poor energy densities [28–31].

Herein, we demonstrate the use of a free-standing, binder-free, mechanically flexible 3D carbon nanotube foam (CNTF) as a scaffold material enabling high sulfur loading with an outstanding electrochemical sulfur utilization of up to 82% at excellent reversibility. Previously reported studies that used carbon-based foams as sulfur hosts involved cumbersome preparation techniques and delivered reasonable electrochemical performance, but poor energy densities [32,33]. The most attractive features of our potential sulfur host are its unique ease of preparation, the absence of any disruptive binder and the dual performance of the electrode as both a sulfur host and a polysulfide trap, which allows high cycling performance of up 1000 cycles. The CNTF is synthesized by a remarkably simple, single-step spray pyrolysis technique using non-toxic ingredients, inspired by the procedure reported by Hashim et al. [34]. With this preparation, we are independent of complex carbon precursors since we mix commonly available reagents such as toluene, ferrocene and a boroorganic compound, which is then spray-pyrolised and the CNTF is directly ready to use after cooling without another purification step. CNTs are linked by the boron species to directly form a CNT-interconnected network without interruption of electrical conduction [34]. The chance for typical exfoliation of the CNTs due to Li^+ ion insertion/removal is rather low. With our material we are able to achieve a high-areal sulfur loading of up to 7.1 $mg_S\ cm^{-2}$ and a sulfur content of 66 wt% within the entire electrode, while still retaining excellent sulfur utilization. To the best of our knowledge, such a facile method of CNTF synthesis leading to an exceptional electrochemical performance has not been reported in the literature so far. The sulfur loading is carried out by simply spreading a calculated amount of commercial sulfur powder on the foam and heating it at 155 °C for one hour, making the whole process completely solvent-free, cost-effective and quick. This method thus enhances its potential to be scaled up by using fairly simple apparatus. The typical foam-like structure enables excellent electrolyte absorbability and may aid in the retention of dissolved polysulfides within the CNTF, thereby enhancing the cycling stability. The interconnected CNT framework offers a long-range conductive network for an efficient electron transport and a high sulfur utilization. We demonstrate electrodes that exhibit areal capacities of ~ 9 mAh cm^{-2} (72% sulfur utilization) at 0.1 C and ~7.5 mAh cm^{-2} (60% sulfur utilization) at 0.2 C rates at extremely low overall electrode weight (800 mAh $g_{electrode}^{-1}$ at 0.1 C). At lower sulfur loadings, the electrodes show an initial discharge capacity of 1378 mAh g_S^{-1} (82% sulfur utilization) and could be cycled 1000 times with an excellent capacity retention of 53.1%.

2. Experimental section

2.1. Synthesis of the CNT foam

The multi-walled CNT foams were synthesized *via* a single-step spray pyrolysis technique by using a precursor solution containing a mixture of 1.25 g ferrocene ($C_{10}H_{10}Fe$, Alfa Aesar, purity: 99.5%) and 0.5 g benzeneboronic acid ($C_6H_7BO_2$, Alfa Aesar, purity: > 98%) in 100 mL toluene (C_7H_8, Merck, purity: > 99.99%). A steady precursor spray was generated with the help of a spray system and the fine spray was carried by argon gas into a horizontal quartz tube, maintained at a temperature of 860 °C. The synthesis was carried out until the precursor solution was exhausted (~ 25 min). Fe in ferrocene acts as a catalyst for the growth of CNTs, whereas toluene serves as the carbon source. Boron, from the benzeneboronic acid, aids in the formation of stable bends in the CNTs and also significantly increases the aspect ratio of the nanotubes, resulting in a mechanically flexible and ultra-light weight, free-standing CNTF, which is collected on the inner walls of the quartz tube [34].

2.2. Sulfur infiltration

The as-synthesized CNTFs were punched in the shape of circular discs of diameter 11 mm. The typical areal mass of the CNTF discs was between 2–4 mg cm^{-2}. A calculated amount of commercial sulfur powder was spread onto the CNT discs as uniformly as possible. Typically, 2–3 mg sulfur was impregnated into the foams, which constituted an areal loading of approximately 2.1–3.2 $mg_S\ cm^{-2}$. Higher sulfur mass loadings of up to 7.1 $mg_S\ cm^{-2}$ were tested as well for determining the practical viability of the cells. The foams were subsequently heated at 155 °C in an Ar flow for one hour.

2.3. Material characterization

SEM images and EDX spectra/elemental mapping results were obtained with a scanning electron microscope (FEI NOVA NANOSEM-200) at 15 kV. Raman measurements were performed by means of a Thermo Scientific DXR Smart Raman Spectrometer with a laser excitation wavelength of 532 nm (2.33 eV) and a power equal to 8 mW. The wetting of the CNTF was studied using a sessile-drop technique as described elsewhere [35,36]. Several pieces of sulfur with a total weight of about 40 mg were stacked onto a piece of CNTF (about

1.5 cm × 1.5 cm), serving as a substrate. Then the substrate with sulfur was set on a molybdenum support situated in a homogeneous temperature zone of a high-temperature chamber of the sessile-drop device. After evacuation of the chamber to about 10^{-5} mbar, it was filled with high purity argon (99.999%) to a pressure of about 900 mbar and heated to a set temperature of 123 °C at a rate of 5 K min^{-1}. The sulfur content in the electrodes was determined by thermogravimetry (STA449C Jupiter, Netzsch) after heating in air from room temperature to 500 °C at a rate of 10 °C min^{-1}. The X-ray diffraction measurements were carried out using an X-ray powder diffractometer from STOE (type Stadi P) performed in transmission geometry with Co $K_{\alpha 1}$ radiation (λ = 1.78896 Å) with curved Ge(111) crystal monochromator. The samples were measured in a range of 5–80° 2θ with a step size of $\Delta 2\theta$ = 0.01°. X-ray photoelectron spectroscopy (XPS) was carried out with a Physical Electronics PHI 5600 CI with monochromated Al K_{α} radiation (λ = 1.4867 keV; 350 W) X-ray source at a pass energy of 29 eV and a step size of 0.1 eV for the hemispherical analyzer. The cycled electrodes were washed with DOL solvent inside the glove box prior to the *ex-situ* SEM/EDXS and XPS investigations. The variation in the thickness of the foam under the influence of external pressure was determined by means of a digital micrometer, Mahr Micromar 40 EWR. The pressure between the two stamps at every point was estimated by placing a certain weight on the CNTF and visually evaluating the thickness of the foam.

2.4. Electrochemical testing

CR2032-type stainless steel coin cells were assembled inside an Ar-filled glovebox with the sulfur-impregnated cathodes and lithium metal anodes separated by a commercial microporous (Celgard 2500, diameter 16 mm) separator. 1 M LiTFSI salt (BASF) in a mixed solvent of 1,3-dioxolane (DOL, Aldrich) and 1,2-dimethoxyethane (Aldrich) (1:1 by volume), with 0.25 M $LiNO_3$ (Merck) as additive, was used as the electrolyte. 80 µL of electrolyte was used in all cells. Lithium metal foil (Chempur, diameter 13 mm, thickness 250 µm) was used as anode material and reference electrode. The cycling tests were performed at room temperature using a BaSyTec cell test system in a potential window of 1.8–2.6 V *vs.* Li/Li^+ at various cycling rates of 0.2–3.2 C, based on the mass and theoretical capacity of sulfur. Cyclic voltammetry and EIS measurements were performed using a VMP3 potentiostat (Bio-logic). The cyclic voltammograms were recorded at a scan rate of 0.1 mV s^{-1} within a potential range of 2.8–1.8 V *vs.* Li/Li^+. EIS measurements were recorded from 200 kHz to 100 mHz with an AC voltage amplitude of 5 mV at the open circuit voltage of the cells.

3. Results and discussion

3.1. Morphology of the as-synthesized CNTF

A typical photograph of the as-synthesized CNTF used in this study is shown in Fig. 1a. Benzeneboronic acid (BBA), present in the precursor mixture, provides boron that aids in the formation of stable bends in the CNTs and also significantly increases the aspect ratio of the nanotubes, resulting in a mechanically flexible and lightweight CNTF. This behavior confirms that the highly flammable component, triethylborane used by Hashim et al. [34], can be replaced with non-harmful BBA without losing the favorable attributes of the CNTF. A schematic of the spray pyrolysis set up used in our study is presented in Fig. S1 (Supporting Information). The volume of the foam synthesized in a batch directly depends on the size of the furnace hot zone, which

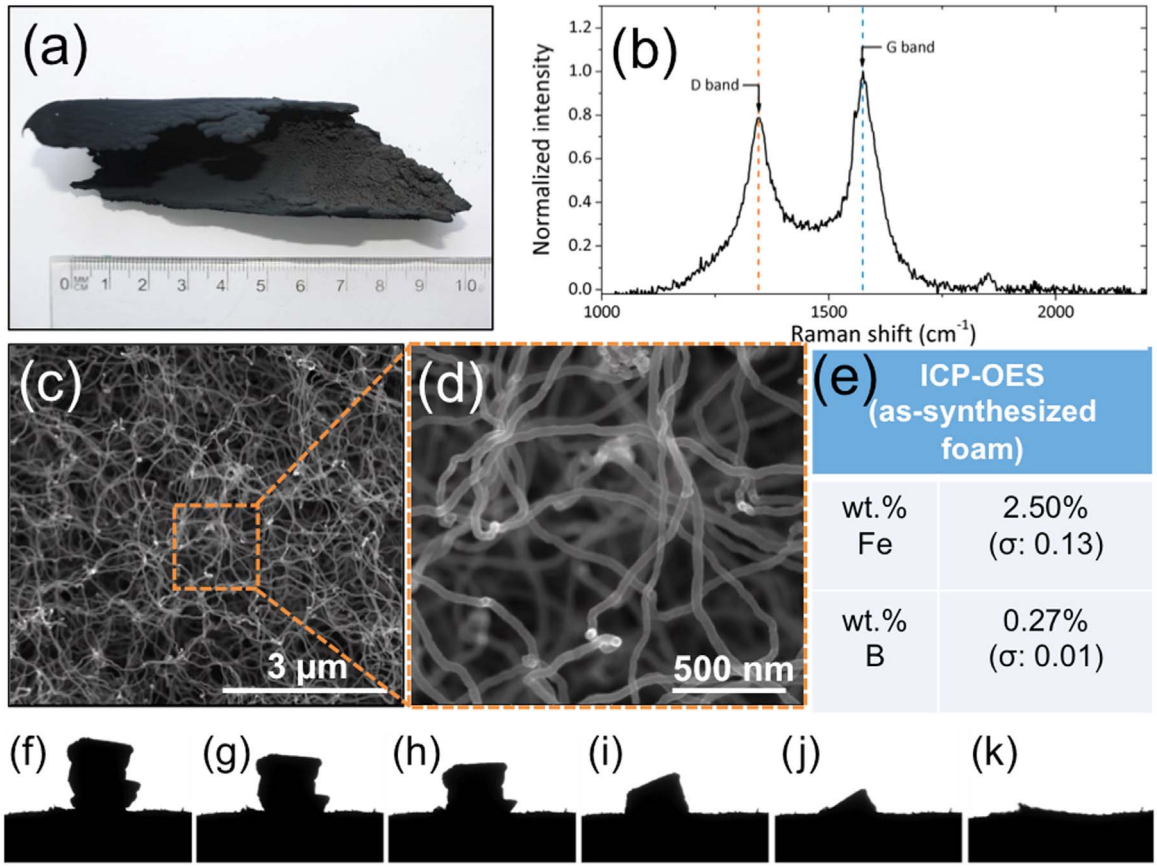

Fig. 1. a) Photograph of the as-synthesized CNTF. b) Raman spectrum of the as-synthesized CNTF. c) SEM image of the interconnected CNT network taken at 15 kV. d) Magnification of the orange squared region in (c). e) Concentration of trace elements (Fe and B) as analyzed by ICP-OES. f-k) Melting and infiltration of sulfur (stacked as sheets) into the CNTF substrate at 123 °C: f) t = 0 s – solid state just before melting; g) t = 21 s; h) t = 1 min 07 s; i) t = 1 min 53 s; j) t = 2 min 23 s; k) t = 4 min 27 s. (For interpretation of the references to color in this figure legend, the reader is referred to the web version of this article).

ensures an easy scale-up of the process. 3D CNTFs as large as 30 cm × 4 cm × 0.1 cm are grown in one batch of synthesis using our apparatus (Fig. S2, Supporting Information). The structure of the CNTs was characterized by Raman spectroscopy and X-ray diffraction (XRD). Fig. 1b presents the Raman spectrum of the as-synthesized CNTF with two peaks at 1345 cm^{-1} (known as the D-band) and 1575 cm^{-1} (known as the G-band), corresponding to the disordered carbon and graphitic (sp^2) carbon, respectively [37]. The intensity ratio of D- and G-bands (I_D/I_G) indicates the degree of graphitization in the CNTs. A ratio of 0.80 is obtained for the CNTs in our study, which is typical for multi-walled CNTs [38]. The scanning electron microscopy (SEM) images of the CNTF, shown in Fig. 1c and d, indicate that the foam is composed of closely spaced entangled nanotubes forming an interconnected network. More images of the CNTF, showing boron-induced elbow junctions are presented in Fig. S2 (Supporting Information). The average diameter of the CNTs is determined as 30 ± 10 nm. The voids between the CNTs vary up to only 1 μm, suggesting that such finely woven network ensures a tight electrical contact with the active material. Simultaneously, the interconnected porosity and flexibility in the foam aid in retaining the electrolyte within the foam and in accommodating volumetric changes during discharging-charging cycles. The concentrations of trace elements, Fe and B present in the as-synthesized CNTs, as analyzed by inductively coupled plasma-optical emission spectrometry (ICP-OES), are shown in Fig. 1e. The content of Fe and B is found to be 2.50 wt% and 0.27 wt%, respectively. The *ex-situ* characterization of the cathode proves later in the article that the concentrations of both Fe and B are low enough to not interfere with the electrochemical reactions.

3.2. Sulfur loading – behavior and morphology during and after infiltration

The high temperature behavior of sulfur on the CNTF substrate was recorded by means of a high-speed/high-resolution charge-coupled

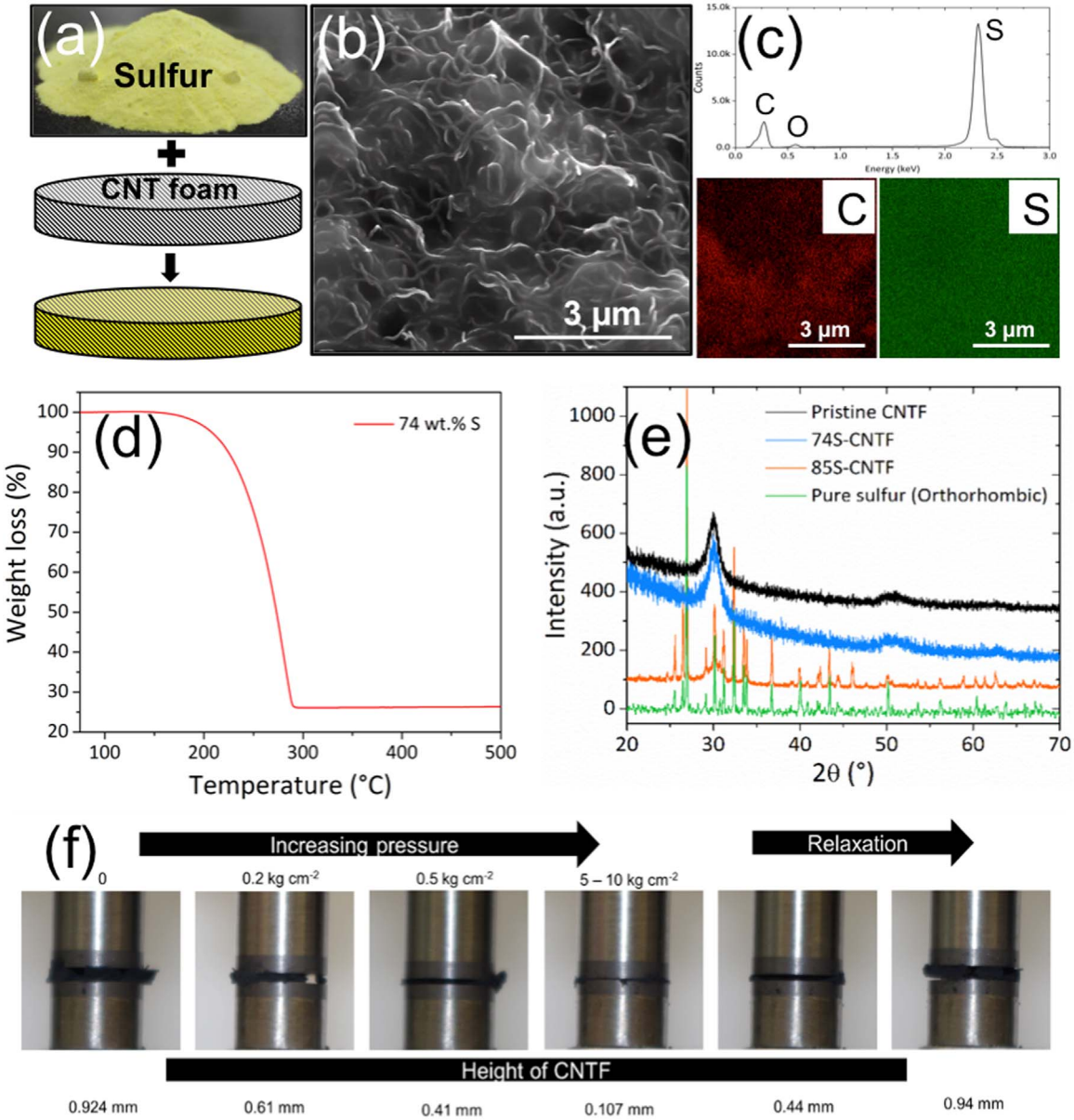

Fig. 2. a) Schematic drawing of sulfur impregnation on the CNTF. b) SEM image of the S-impregnated CNTF. c) EDX spectrum and mapping of sulfur and carbon species in the S-impregnated CNTF. d) TG profile of the 74 wt% S-containing CNTF (74S-CNTF electrode). e) XRD patterns of pristine and S-impregnated CNTFs (Intensities of the spectra from 85S-CNTF and pure sulfur were reduced by ⅓rd and increased by five times, respectively, for the sake of comparison). f) Variation of the thickness of the CNTF at different pressures reasonably present in coin cells.

device (CCD) camera. As observed from a series of digital images in Fig. 1(f-k) and the corresponding video in the Supporting Information, sulfur began melting upon approaching the set temperature of 123 °C and the molten species immediately started to penetrate the substrate. It took about 4.5 min to completely infiltrate into the substrate (note: the video is compressed on the time scale). Fig. S3 (Supporting Information) presents an SEM image of the S-impregnated CNTF after the wettability test showing no hints of large sulfur particles, which supports excellent wettability of the CNTF material.

CNTF electrodes are simply punched out from the as-synthesized sheet in the required diameter, 11 mm in our case, for impregnation with sulfur. As illustrated in Fig. 2a, commercial sulfur powder is spread uniformly on the foam, which is subsequently heated in Ar at 155 °C for one hour. The entire process of synthesis and impregnation are thus very simple, solvent-free and quick compared to the complex methods reported in literature [11,13–16]. The principal advantages of our preparation technique are: (i) the spray pyrolysis allows for a high throughput of as-produced materials as compared to thermal chemical vapor deposition, (ii) the technique can relatively easily be scaled up, (iii) very little unwanted species are obtained (e.g. amorphous carbon) and (iv) the technology is simple, cost-effective and reliable as our system does not employ radio frequency sonication and can be operated at atmospheric pressure. SEM measurements were performed to characterize the sulfur-impregnated foam in order to reveal the dispersion state of sulfur, which is crucial to the electrochemical performance of the electrode. The SEM image, shown in Fig. 2b, indicates that sulfur is uniformly embedded within the CNT network without agglomerations. The 3D structure and the associated voids in the CNTF, which are still intact after impregnation, can accommodate volume changes during cycling and also allow for efficient electrolyte penetration, thus facilitating Li^+ ion transport and consequently improving the electrode kinetics. Energy dispersive X-ray spectroscopy (EDXS), shown in Fig. 2c, demonstrates a high S peak and that C and O exist in the electrode. The EDXS mappings of sulfur and carbon corroborate that sulfur is uniformly distributed within the CNTF, maintaining good contact with the conductive network, which is particularly desirable for high sulfur utilization during the electrochemical redox processes. The mass of active material in the electrode was characterized by thermogravimetric analysis (TGA). The TGA curve, shown in Fig. 2d, obtained from a S-impregnated CNTF indicates a continuous weight loss between 150–290 °C, corresponding to the oxidation of sulfur in air. We observed that sulfur loadings as high as 85 wt% may result in the formation of locally confined large crystallites or agglomerates, which is suggested by the presence of characteristic sulfur reflections in the X-ray diffraction (XRD) pattern of the CNTF impregnated with 85 wt% sulfur ('85S-CNTF' electrode), indexed with the structure model with *Fddd* space group, as shown in Fig. 2e. Such agglomerates may not be effectively linked to the conductive CNT framework and readily dissolve in the electrolyte causing adverse effects on the cycling performance. Ma et al. observed similar behavior of their cells when the mass loading of sulfur exceeded 70 wt% [39]. XRD patterns of pristine- and 74S-CNTF (74 wt% sulfur) are also shown in Fig. 2e, both showing no characteristic sulfur peaks. The two reflections at 30.2° and 50.3° correspond to the graphitic planes (002) and (100), respectively from the nanotubes [40]. The absence of reflections corresponding to crystalline sulfur in the 74S-CNTF electrode reveals that sulfur is in a highly dispersed amorphous state, not detectable by XRD but clearly verified by EDXS [26,41,42]. Hence, the maximum sulfur loading is restricted to less than 74 wt% in our study. Typically, the foams are impregnated with 0.9–7.1 $mg_S\ cm^{-2}$, corresponding to 20–66 wt% for electrochemical studies.

We also considered the porosity of our CNTF and the utilization of void space in our CNTF, which is a very important parameter to achieve high volumetric density for automotive applications and to reduce the amount of electrolyte within the cell [43]. The dead volume within the electrode should be as low as possible for efficient use of electrolyte and volume within the cell. With a height of 1000 μm and a sulfur ratio of 66 wt%, the filling of the volume within the foam corresponds to just 4% considering a density of 2.07 $g\ cm^{-3}$ for sulfur and 1.8 $g\ cm^{-3}$ for carbon. Hence, the utilization of void space within the foam seems to be too low for any application. However, by applying a little external pressure on the foam of less than 1 bar, which is far lower than what is exerted in coin cells, the height of the foam was reduced from 1000 μm to roughly 150 μm without changing the integrity of the foam. With the release of pressure, the foam expanded rapidly to its initial height. This fact implies that the empty volume within the final cell will be reduced from 96% to less than 50% depending on the pressure within the coin cell. For demonstration, Fig. 2f shows the extent of shrinkage of CNTF as a function of external load. The CNTF shrinks to about 11.6% of its initial value under a certain pressure, considerably increasing the volumetric energy density. Hence, the porosity of the material can be tailored to achieve high volumetric energy densities also. In addition, the amount of electrolyte in the cell can be reduced to a specific volume of at least 11 $\mu L\ mg_S^{-1}$, which will be demonstrated in the next section.

3.3. Electrochemical testing in half-cell setup

The electrochemical performance of Li-S cells assembled in CR 2032 coin cells with a 33S-CNTF cathode (33 wt% sulfur, corresponding to a mass loading of 2 $mg_S\ cm^{-2}$) was evaluated by conducting cyclic voltammetry (CV), electrochemical impedance spectroscopy (EIS), cycling and C-rate tests. Firstly, the electrochemical kinetic process was studied by means of cyclic voltammograms, as shown in Fig. 3a, obtained by cycling the cells in between 2.8 to 1.8 V at a scan rate of 0.1 $mV\ s^{-1}$. The two reduction peaks at 2.28 and 1.96 V during the first cathodic scan represent a typical two-step reduction of elemental sulfur to high-order polysulfides (Li_2S_x; $8 \geq x \geq 4$) and then to low-order polysulfides (Li_2S_x, $x \leq 4$) and Li_2S_2/Li_2S, respectively [27,44]. The small hump at 2.15 V seen only during the first cathodic scan may be attributed to the conversion of high-order polysulfides to medium-order polysulfides (Li_2S_6 to Li_2S_4), which is associated with the main peak at 1.96 V [10,45]. The subsequent anodic sweep accompanies two distinguishable peaks at 2.34 and 2.45 V representing backward transition from Li_2S_2/Li_2S to low-order polysulfides and eventually to elemental sulfur [20]. Along the successive cycles (2nd, 10th and 30th), the overpotential reduces, which is possibly explained by the occurrence of a conditioning process where rearrangement of the active material to more electrochemically favorable sites occurs within the 3D CNT scaffold. A good overlap of the cathodic peaks along the 2nd to 30th cycles suggests that the CNTs maintain an intimate contact with the active material and effectively aid in faster electron kinetics and enhanced Li^+ ion diffusion. Furthermore, it may be reasoned that the excellent electrochemical stability is caused by reduced polysulfide shuttling by the tight network of CNTs. The cells are further subjected to 200 discharging-charging cycles between 2.6 and 1.8 V at a C-rate of 0.2 C and the corresponding voltage profiles are shown in Fig. 3b, for cycle nos. 1, 10, 50, 100 and 200. All the curves are consistent with the CV curves. The discharging curves are composed of two plateaus, the upper plateau (~2.35 V) corresponding to the transformation of sulfur/high-order polysulfides to low-order polysulfides and the lower plateau (~2.08 V) representing the final transformation into solid Li_2S_2/Li_2S, which are revisited in the charging plateaus for the backward reactions as well. There is no significant increase in the overpotential between the 1st (ΔE = 145 mV) and the 200th (ΔE = 150 mV) cycles, which is ascribed not merely to the enduring contact between the conductive CNTs and sulfur, but also to the role of the CNTF in acting as a reservoir for trapping soluble lithium polysulfides for reutilization. Fig. S4 (Supporting Information) shows a comparison of the cycling performance of two CNTF electrodes with similar sulfur mass loadings (~7.2 $mg_s\ cm^{-2}$), one with a commercial separator and the other with a modified separator in order to

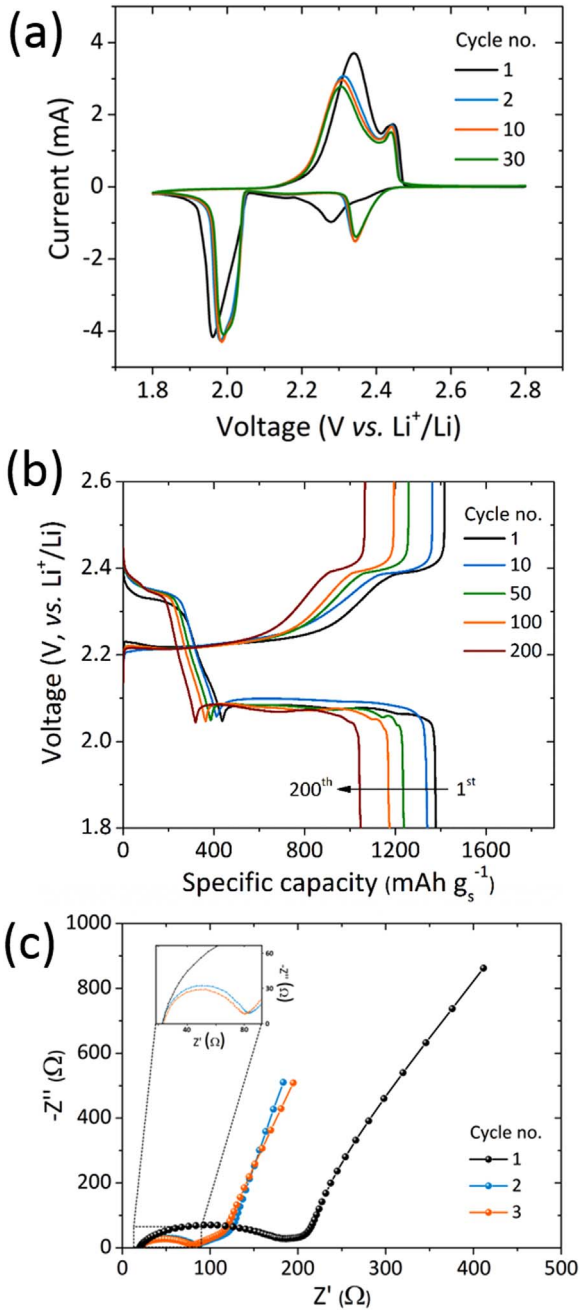

Fig. 3. a) CV profiles recorded at 0.1 mV s^{-1}. b) Voltage profiles for discharging-charging cycles (cycle nos. 1, 10, 50, 100, 200) at a C-rate of 0.2 C. c) Comparison of the electrochemical impedance spectra for the three initial cycles of the 33S-CNTF electrode.

suppress polysulfide diffusion to the anode [21,22]. The cycling behavior remains the same in both cases, suggesting that the electrode itself may possess the favorable characteristics of the mesoporous carbon-coated separator in trapping soluble lithium polysulfide species. Electrochemical impedance spectroscopy (EIS) was conducted to obtain further insights into the internal resistance and charge-transfer processes of the electrodes. The Nyquist plots for the three initial cycles, shown in Fig. 3c, reveal a single semicircle at high-to-medium frequency region and an inclined line at the low frequency region, which correspond to the charge transfer resistance (R_{CT}) and mass transfer processes, respectively [46]. A high charge transfer resistance of 151 Ω is evident for the 1st cycle, followed by a rapid decline to approximately 55 Ω for the 2nd and the 3rd cycle, which may be attributed to a more efficient Li^+ ion diffusion into the 3D cathode due to better wetting and electrolyte penetration in the subsequent cycles.

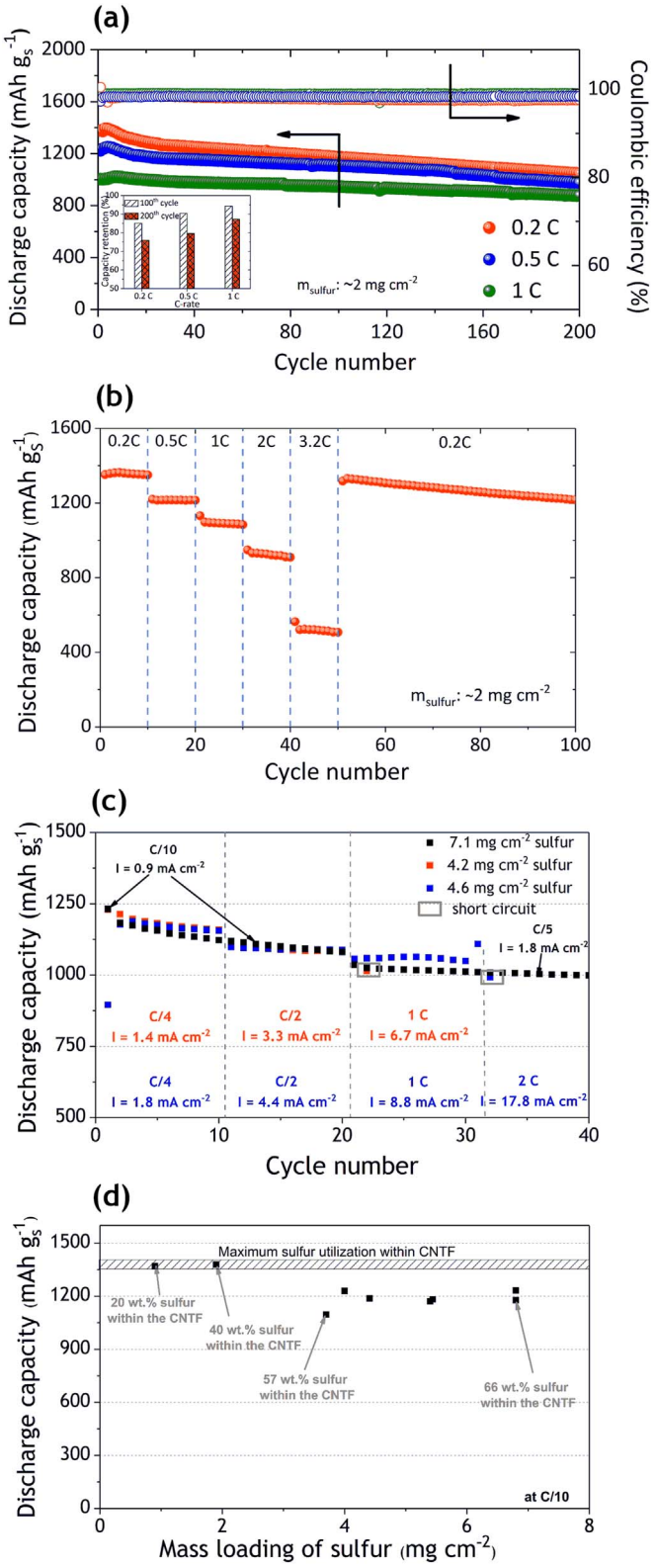

Fig. 4. a) Cycling performances of the 33S-CNTF electrode at 0.2 C, 0.5 C and 1 C. b) Rate performance of the Li-S cell with 33S-CNTF electrode. c) Rate tests of the S-CNTF at different sulfur loadings. At high current rates of 7–18 mA cm^{-2} the lithium dendrites grow extremely fast and cause a short circuit of the cell. d) Effect of sulfur mass loading on the initial discharge capacity at a current rate of C/10.

The redistribution of sulfur species to more electrochemically favorable positions within the conductive foam further minimizes the barrier of electron transfer and promotes Li^+ ion diffusion. The charge transfer

resistance is quite low, especially after the first cycle, which is consistent with the values reported in literature for similar cathode systems [25,47].

The cycling performance of the 33S-CNTF electrode (areal sulfur loading: ~2 $mg_S\ cm^{-2}$) at different C-rates is shown in Fig. 4a. The initial discharging capacities at 0.2 C, 0.5 C and 1 C are 1379, 1225 and 1004 mAh g_S^{-1}, respectively. After 200 cycles, the discharging capacities are as high as 1046, 975 and 877 mAh g_S^{-1}, corresponding to capacity retentions of 75.8%, 79.6% and 87.3%, respectively. The capacity retention at different C-rates after 100 and 200 cycles are compared in the inset of Fig. 4a.

The phenomenal capacity retention of the Li-S cells over 200 cycles may be ascribed to the alleviated active material loss due to effective trapping of the electrolyte containing dissolved polysulfides and their reutilization within the interconnected foam-like CNT scaffold. It is noticed that as the C-rate increases from 0.2 C to 1 C, both the capacity retention and Coulombic efficiency after 200 cycles increase from 75.8 to 87.3% and 97.8 to 99%, respectively. This behavior is caused by the higher discharging-charging rates, which weaken the shuttle effect of dissolved polysulfides by reducing their retention time in the electrolyte per cycle [6]. The polysulfides are thereby excluded from the kinetically controlled parasitic reactions, consequently suggesting that higher C-rates are more favorable for practical applications. An apparent slight increase in the capacity for the first few cycles for all C-rates may be attributed to a gradually increased sulfur participation in the electrochemical reactions, which is a common phenomenon for electrodes with a high sulfur mass loading [48]. It is further evident that the maximum discharging capacities at the C-rates 0.2 C, 0.5 C and 1 C occur at 3rd (1391 mAh g_S^{-1}), 4th (1250 mAh g_S^{-1}) and 7th (1021 mAh g_S^{-1}) cycle, respectively, which indicates that the maximum sulfur participation in the electrodes is delayed as the C-rate increases. By the completion of the 200th cycle, the discharging capacities of the Li-S cells at 0.2 C, 0.5 C and 1 C remained at 1046, 975 and 877 mAh g_S^{-1}, respectively, corresponding to low capacity fading rates of 0.120%, 0.102% and 0.063% per cycle, respectively, thus demonstrating an excellent cycle stability. In order to further investigate the rate capability of the 33S-CNTF electrode, the Li-S cells were discharged-charged at various current densities from 0.2 to 3.2 C (1 C = 1672 mA g_S^{-1}), for 10 cycles at each C-rate. As presented in Fig. 4b, the cells exhibit stabilized discharging capacities of 1350, 1215 and 1084 mAh g_S^{-1} at the end of the last cycle at each C-rate, 0.2 C, 0.5 C and 1 C, respectively. Even at higher C-rates of 2 C and 3.2 C, the cells deliver high capacities of 909 and 507 mAh g_S^{-1} respectively at the end of the last cycle. Given that no modifications such as porous carbon membranes or interlayers are used in this cell configuration, these values are very promising [21,22]. Furthermore, in our study, an excellent reversible capacity of 1318 mAh g_S^{-1} is recuperated when the C-rate is reset to 0.2 C, which is only marginally lower than that of the initial 10 cycles at 0.2 C, implying high reversibility of the S-impregnated 3D CNT electrode. Moreover, the subsequent 50 cycles (from cycle no. 50 to 100) at 0.2 C demonstrated only minor capacity fading. The high rate capability is attributed to enhanced electrode kinetics resulting from the interconnected porous network of the S-impregnated CNT electrode as shown in Figs. 2b and c [49]. Further tests conducted, as shown in Fig. 4c, clearly reveal that even at high current densities of 17 mA cm^{-2} and an areal mass loading of 4.6 $mg_S\ cm^{-2}$ sulfur, the capacity is still around 1000 mAh g_S^{-1} which, when compared to literature, is an outstanding value (see Table 1 for comparison). However, the cell fails immediately during charging as the lithium dendrites pierce through the separator and cause short circuits. Note that at high current densities the growth of lithium dendrites on the anode is extremely fast and typically causes cell failure within a few cycles. [50] This dramatic issue is independent of the structure of the sulfur cathodes and can only be prevented by the use of advanced separators, modified electrolytes or alternative anodes, which is out of scope for the present study. Interestingly, current densities of up to 8.8 mA cm^{-2} hardly affect the capacity even at sulfur loadings of up to 4.6 $mg_S\ cm^{-2}$ and only cause a drop of less than 10% compared to the capacity at a low current density of 1.8 mA cm^{-2}.

In order to further evaluate the effect of the sulfur mass loading on the capacity, we developed a function of specific capacity in relation with sulfur mass loading (Fig. 4d) at a C-rate of C/10. At low sulfur loading (< 2 $mg_S\ cm^{-2}$), a capacity of up to 1400 mAh g_S^{-1} is obtained, which represents the maximum utilization of sulfur possible within the CNTF. Increasing the sulfur loading to about 4 $mg_S\ cm^{-2}$ (57 wt%) causes a drop to about 1200 mAh g_S^{-1} as a result of more electrically insulated sulfur within the electrode. Interestingly, almost no further capacity drop is observed when the sulfur loading is raised to 7 $mg_S\ cm^{-2}$, thus highlighting the extremely good electrical conductivity of the CNTF.

The long-term cycling performance of Li-S cells with 19S-CNTF (0.9 $mg_S\ cm^{-2}$) cathode was tested at a current rate of 0.2 C, as shown in Fig. 5a. We adopted relatively low sulfur loading in order to avoid a cell failure caused by lithium dendrite growth and electrolyte depletion, which typically occurs very fast at high areal capacities. With an initial discharging capacity of 1344 mAh g_S^{-1}, the cells show a remarkable cycling stability advancing to 1000 cycles. Moreover, the Coulombic efficiency for the first few cycles is as high as 98.8% and thereafter remained at ~ 99.4% until the end of the 1000th cycle, suggesting that the desirable role of the 3D CNTF electrode in capturing the dissolved polysulfides remains active even after exhaustive cycling for up to 1000 cycles. The discharging capacity at the end of the 1000th cycle remains at 713 mAh g_S^{-1}, suggesting a capacity fading rate of only 0.047% per cycle, which is outstanding and comparable to some of the recently achieved values in the literature [25].

As a next step, the sulfur mass was increased substantially. High sulfur loadings are extremely important when it comes to practical applications i.e. for automotive applications, but it typically lowers the electrochemical performance making most electrode designs unfeasible for commercial use [51]. In order to investigate whether our concept is transferable for

Table 1
Comparison of the electrochemical performance of the 3D CNT foam used in the present study with Li-S cells reported in the literature, using free-standing carbon nanotube (CNT)-based cathode hosts.

Host	Areal sulfur mass loading (mg cm^{-2})	Areal capacity (mAh cm^{-2})	Specific capacity total mass of electrode (mAh $g_{electrode}^{-1}$)	Capacity fading per cycle	Reference
3D carbon fabric	6.50	5.3 (at 0.1 C)	342 (at 0.1 C)	1.22% (over 50 cycles)	[57]
GDL-CNT	6.90	3.3 at (0.1 C)	220 (at 0.1 C)	6.60% (over 12 cycles through 0.05 C to 0.3 C)	[56]
3D CNT paper	6.3 (single layer)	6.2 (at 0.05 C)	540 (at 0.05 C)	0.20% (over 150 cycles at 0.05 C)	[58]
MWCNT paper	2.3	3.3 (at 0.2 C)	770 (at 0.2 C)	0.13–0.24% (over 100 cycles at 0.2 C)	[59]
CNT film	3.7	3.1 (at 0.5 C)	552 (at 0.5 C)	0.043% (over 500 cycles at 0.5 C)	[60]
CNT film	3.21	3.53 (at 0.1 C)	710 (at 0.1 C)	0.19% (over 100 cycles at 0.1 C)	[61]
3D CNT foam	7.1	9.00 (at 0.1 C)	800 (at 0.1 C)	0.20% (over 167 cycles through 0.1 C to 0.2 C)	Our results

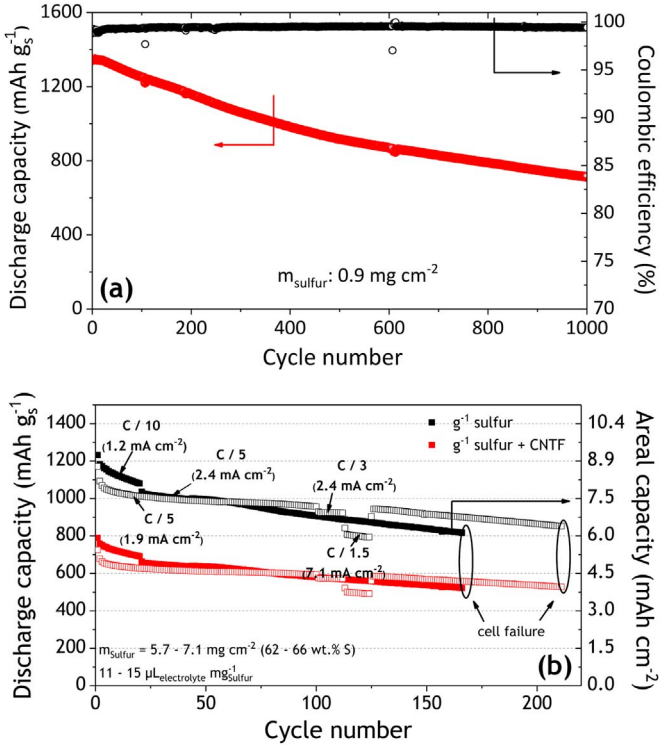

Fig. 5. Long-term GCPL experiments of a) a cell with a low areal mass loading of 0.9 mg$_S$ cm^{-2} at 0.2 C. b) Two cells with higher areal mass loading of 5.7 mg$_S$ cm^{-2} (□) and 7.1 mg cm^{-2} (■) at different current densities.

high energy and high power application such as automotive use, we tested our S-CNTFs under practical conditions with high sulfur loadings and relatively low electrolyte amount. Fig. 5b shows the results obtained from further long-term experiments conducted with higher sulfur loadings (5.7–7.1 mg$_S$ cm^{-2}). After 100 cycles with 5.7 mg$_S$ cm^{-2}, the current density was increased from 1.9 mA cm^{-2} to 7.1 mA cm^{-2}, which resulted in a capacity drop of about 15% only. Immediately after reducing the current density, the capacity recovered to about 950 mAh g$_S^{-1}$. A cell failure is observed after 210 cycles for the cell with a sulfur mass loading of 5.7 mg$_S$ cm^{-2}, which is slightly delayed compared to the other cell (with a mass loading of 7.1 mg$_S$ cm^{-2}) due to a lower sulfur loading and a higher electrolyte/sulfur ratio (15 µl mg$_S^{-1}$) in the former case. These results are in good agreement with the observations of Thieme et al. [52] and demonstrate the outstanding physical properties of the CNTF.

The cycling performance of the cell with a sulfur mass loading of 7.1 mg$_S$ cm^{-2} shown in Fig. 5b contains an specific electrolyte volume of 11 µL mg$_S^{-1}$. A high areal capacity of ~9 mAh cm^{-2} (800 mAh g$_{electrode}^{-1}$) and still about 7 mAh cm^{-2} at 0.2 C are achieved along with good cycling stability. After 150 cycles at 0.2 C, the areal capacity is still as high as 6.2 mAh cm^{-2}. Note that 4 mAh cm^{-2} is considered to be sufficient for automotive applications [53]. At the 167th cycle, cell failure has occurred because of the growth of lithium dendrites piercing through the separator or electrolyte depletion [51,54]. With a better anode (e.g., a lithiated silicon anode) [55] and/or a more mechanically stable separator, more cycles at higher sulfur mass loading could be achieved, but this is out of scope for this study.

We compared our results at high sulfur loading to the existing literature on similar systems. Hagen et al. also tested CNT-coated carbon current collectors (GDL) and infiltrated with sulfur under similar conditions. They obtained about 700 mAh g$_S^{-1}$ and 220 mAh g$_{electrode}^{-1}$, respectively (3.3 mAh cm^{-2}), at 0.1 C with a mass loading comparable to ours (6.9 mg$_S$ cm^{-2}) [56]. In a further work of their group, the sulfur utilization was increased to 1000 mA g$_S^{-1}$ at about 0.1 C with an areal capacity of 8 mAh cm^{-2} and a total specific capacity of 400 mAh g$_{electrode}^{-1}$ [43]. At comparable conditions, we obtained twice of the total specific capacity with about 800 mAh g$_{electrode}^{-1}$ (Fig. 5b). Han et al. tested a 3D carbon fabric network infiltrated with sulfur (6.5 mg$_S$ cm^{-2}) at about 0.1 C and obtained maximum 820 mAh g$_S^{-1}$ followed by a rapid degradation to less than

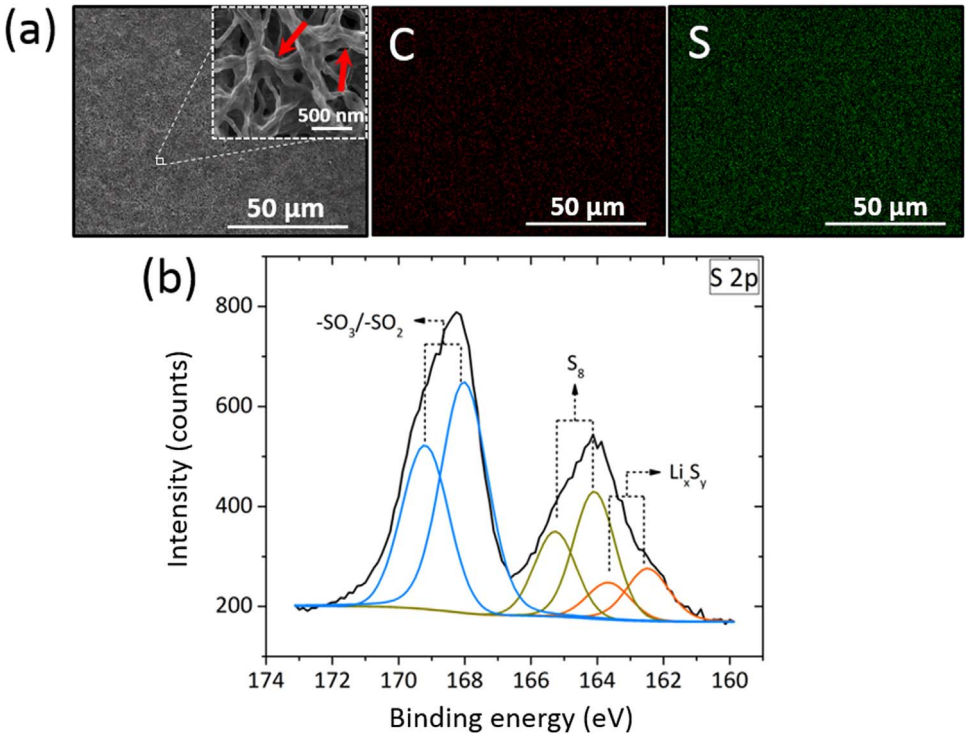

Fig. 6. a) SEM image of the 33S-CNTF electrode (~2 mg$_S$ cm^{-2}) at the end of the 200th cycle (Inset shows a higher magnification image) and the EDXS elemental mappings of the sulfur and carbon species. b) High-resolution S 2p XP spectra of the cycled S-impregnated CNTF electrode. The black line corresponds to the experimental data and the colored lines correspond to the deconvolution of various species.

400 mAh g_S^{-1} after 50 cycles [57]. Yuan et al. [58] also prepared free-standing CNT-foams through a slurry based process and obtained an initial areal capacity of 9.4 mAh cm^{-2} (10.9 mg_S cm^{-2}, 54 wt% sulfur ratio at C/20) which is also comparable to our results with 9.0 mAh cm^{-2} (Fig. 5b). However, their sulfur loading and the entire electrode mass was higher up to 45% and 75%, respectively at half of the C-rate used herein considerably reducing the overall energy density compared to our set-up. Table 1 demonstrates the significance of our results in comparison to the existing and recent literature reports. So far we obtained one of the highest specific capacities (800 mAh $g_{electrode}^{-1}$) based on the total electrode mass (incl. current collector) at viable conditions. These results clearly highlight that the superior conductive properties of our novel free-standing CNT foam are the most important and can only be achieved without the use of any binder or substrate. Overall, the cycling stability and areal capacity of our cells are far superior than those obtained by others using similar cathode systems comprising 3D CNT hosts [59–61]. Further, the scope for scalability of the 3D CNT hosts reported therein is extremely limited compared to the solvent-free facile method adopted in our study. Additionally, the specific energy density of our novel cell with 7.1 mg_S cm^{-2} presented in Fig. 5b was determined to be 171 Wh kg^{-1} (U ~ 2.1 V) at 0.1 C in the first cycle including all cell components except the coin cell casing. After 150 cycles at 0.2 C we can still determine 121 Wh kg^{-1}. These values are already excellent results comparable to commercial Li-ion batteries notably considering that we did not optimize the cell components at all (electrolyte amount, lithium metal anode, separator, cathode design and electrode design such as electrode coating on both sides). Overall, the electrochemical performance of the sulfur-impregnated 3D CNTF electrode proves to be quite promising, especially considering that the synthesis is performed *via* a simple, single-step and solvent-free method that can be conveniently scaled up.

In an attempt to shed light on the physical changes occurring on the S-CNTF during electrochemical cycling, *ex-situ* SEM-EDXS and XPS investigations have been conducted on the electrodes that are washed and dried in the charged state. The CNTF cathode, retrieved from the Li-S cells cycled 200 times at 0.2 C, appeared to retain its shape and form, with no visible macroscopic cracks. Fig. 6a shows an SEM image of the cycled foam at lower and higher magnifications. The foam developed no conspicuous cracks or fissures even after 200 cycles and sulfur still appears to be uniformly distributed, as corroborated by the EDX spectra shown for S and C in Fig. 6a. The 3D interlaced CNT electrode remains structurally robust even after long cycling periods. As demonstrated in the higher magnification SEM image (inset of Fig. 6a), sulfur species forms a homogenous coating of 20–70 nm around individual nanotubes (as pointed out by the red arrows). Such morphology suggests that the active material is (i) initially attached to the carbon nanotubes as a uniform coating, ensuring a steady electrical contact for an efficient electron transport, (ii) available in plenty for further discharging/charging reactions and (iii) uniformly distributed within the CNTF and is still closely attached to the tube body even after 200 cycles. Moreover, the pores within the foam, still prevalent after numerous cycles, act as a reservoir for holding electrolyte and also allow for volumetric changes during charging (Fig. S5, Supporting Information).

XPS of the CNT-foam before cycling (Fig. S6, Supporting Information) shows the typical elemental sulfur binding energy doublet at around 164 eV separated into two spectral lines with maxima at 163.8 eV for S $2p_{3/2}$ and 165 eV for S $2p_{1/2}$ due to the spin-orbit-coupling of the S 2p orbital with a band splitting of ΔE = 1.2 eV. After cycling (Fig. 6b) the elemental sulfur is clearly retained since the peak at around 164 eV is still present. Also some traces of lithium polysulfides at around 163 eV seem to be present. The additional signal at binding energies of 168.3 eV results from the conductive salt (Li-TFSI) or from oxidized sulfur species as result of reaction with $LiNO_3$ [62].

4. Conclusions

In summary, we demonstrate the use of a mechanically flexible, binder-free, free-standing 3D carbon nanotube foam with a boron compound as tube connector, synthesized by a simple spray pyrolysis technique involving no harmful chemicals/methods, as a scaffold for high energy Li-S cells. Sulfur impregnation is carried out *via* an inexpensive, solvent-free route without the need of additional purification/surface modification steps, which offers a great advantage over the complex methods reported in literature [11,13–16]. The interlaced CNT network provides highly conductive pathways enhancing electron transport and redox kinetics. The CNTF further restrains the negative polysulfide species and improves electrolyte absorbability, thus suppressing the polysulfide shuttle and minimizing the loss of active material. These appealing characteristics of the CNTF render the S-impregnated CNT cathodes with a high specific capacity, excellent rate capability and a long cycle life. The CNTF exhibits a high intake of sulfur, up to 7.1 mg_S cm^{-2} accounting to 66 wt% in the electrode composite. At lower mass loadings, the electrodes show high initial discharging capacities of 1379, 1225 and 1004 mAh g_S^{-1} at 0.2 C, 0.5 C and 1 C, respectively, with excellent capacity retentions after 200 cycles. The cells further display a superior rate capability of 507 mAh g_S^{-1} at 3.2 C. At much lower mass loadings, the cells are able to exhibit excellent cycling stability for 1000 cycles at 0.2 C with initial and final capacities of 1344 mAh g_S^{-1} and 713 mAh g_S^{-1}. At a higher sulfur mass loading of 7.1 mg_S cm^{-2}, the cells achieve excellent areal capacities of ~9 mAh cm^{-2} at 0.1 C at extremely low electrode weight (800 mAh $g_{electrode}^{-1}$) while still exhibiting excellent reversibility. Such high areal capacities are hardly reported yet for Li-S battery cathodes fabricated using a simple, single-step and scalable method [47]. The specific energy density of our test cell was determined to be 171 Wh kg^{-1} (excluding the cell casing) even without optimization of other cell components or presence of any favorable dopants. Boron is not considered as dopant to influence surface properties but only as CNT “elbow” junction mediator [34]. These considerations clearly highlight the large potential of our cathode, which is readily able to compete with other composites based on reduced graphene oxide [63,64], carbon fibers [65] or multicarbon composite materials [66]. On the whole, our findings pave way for the realization of a cost-effective, facile and commercially viable method of fabricating high-energy Li-S batteries with high sulfur areal loading.

Acknowledgments

The authors would like to thank Mrs. Andrea Voss for the ICP-OES analysis and Mrs. Cornelia Geringswald for the TGA measurements. We would also like to thank Dr. S. Mühlenhoff, Dr. M. Klose and Ms. M. Martine for their invaluable assistance and discussions. Financial support by the German Ministry of Education and Research (BMBF) is gratefully acknowledged under grant no. 01DH14002 (ADNAMSES). Dr. R. Nowak and Prof. N. Sobczak acknowledge financial support from the Foundry Research Institute (Project no. 3604/00).

Appendix A. Supporting information

Supplementary data associated with this article can be found in the online version at doi:10.1016/j.ensm.2017.04.004.

References

[1] P.G. Bruce, S.A. Freunberger, L.J. Hardwick, J.-M. Tarascon, Nat. Mater. 11 (2012) 19.
[2] D.W. Wang, Q.C. Zeng, G.M. Zhou, L.C. Yin, F. Li, H.M. Cheng, I.R. Gentle, G.Q.M. Lu, J. Mater. Chem. A 1 (2013) 9382.
[3] M. Yu, R. Li, M. Wu, G. Shi, Energy Storage Mater. 1 (2015) 51.
[4] J. Shim, K.A. Striebel, E.J. Cairns, J. Electrochem. Soc. 149 (2002) A1321.
[5] J.R. Akridge, Y.V. Mikhaylik, N. White, Solid State Ion. 175 (2004) 243.

[6] Y.V. Mikhaylik, J.R. Akridge, J. Electrochem. Soc. 151 (2004) A1969.
[7] X. Ji, L.F. Nazar, J. Mater. Chem. 20 (2010) 9821.
[8] A. Manthiram, Y. Fu, Y.-S. Su, Acc. Chem. Res. 46 (2013) 1125.
[9] X. Ji, K.T. Lee, L.F. Nazar, Nat. Mater. 8 (2009) 500.
[10] G. Zhou, D.-W. Wang, F. Li, P.-X. Hou, L. Yin, C. Liu, G.Q. Lu, I.R. Gentle, H.-M. Cheng, Energy Environ. Sci. 5 (2012) 8901.
[11] L. Zeng, F. Pan, W. Li, Y. Jiang, X. Zhong, Y. Yu, Nanoscale 6 (2014) 9579.
[12] J.-Q. Huang, Q. Zhang, F. Wei, Energy Storage Mater. 1 (2015) 127.
[13] Y. Zhao, F. Yin, Y. Zhang, C. Zhang, A. Mentbayeva, N. Umirov, H. Xie, Z. Bakenov, Nanoscale Res. Lett. 10 (2015) 450.
[14] M. Wu, Y. Cui, Y. Fu, ACS Appl. Mater. Interfaces 7 (2015) 21479.
[15] L. Zhu, H.J. Peng, J. Liang, J.Q. Huang, C.M. Chen, X. Guo, W. Zhu, P. Li, Q. Zhang, Nano Energy 11 (2015) 746.
[16] L. Sun, D. Wang, Y. Luo, K. Wang, W. Kong, Y. Wu, L. Zhang, K. Jiang, Q. Li, Y. Zhang, J. Wang, ACS Nano 10 (2016) 1300.
[17] N. Jayaprakash, J. Shen, S.S. Moganty, A. Corona, L.A. Archer, Angew. Chem. 123 (2011) 6026.
[18] J. Hassoun, B. Scrosati, Adv. Mater. 22 (2010) 5198.
[19] L. Suo, Y.-S. Hu, H. Li, M. Armand, L. Chen, Nat. Commun. 4 (2013) 1481.
[20] Y.S. Su, A. Manthiram, Chem. Commun. 48 (2012) 8817.
[21] J. Balach, T. Jaumann, M. Klose, S. Oswald, J. Eckert, L. Giebeler, Adv. Funct. Mater. 25 (2015) 5285.
[22] J. Balach, T. Jaumann, M. Klose, S. Oswald, J. Eckert, L. Giebeler, J. Phys. Chem. C 119 (2015) 4580.
[23] C. Liang, N.J. Dudney, J.Y. Howe, Chem. Mater. 21 (2009) 4724.
[24] W. Wei, J. Wang, L. Zhou, J. Yang, B. Schumann, Y. NuLi, Electrochem. Commun. 13 (2011) 399.
[25] R. Fang, S. Zhao, P. Hou, M. Cheng, S. Wang, H.M. Cheng, C. Liu, F. Li, Adv. Mater. 28 (2016) 3374.
[26] R. Elazari, G. Salitra, A. Garsuch, A. Panchenko, D. Aurbach, Adv. Mater. 23 (2011) 5641.
[27] S. Thieme, J. Brückner, I. Bauer, M. Oschatz, L. Borchardt, H. Althues, S. Kaskel, J. Mater. Chem. A 1 (2013) 9225.
[28] Z. Li, J. Zhang, B. Guan, D. Wang, L.M. Liu, X.W.D. Lou, Nat. Commun. 7 (2016) 13065.
[29] X. Wang, G. Li, J. Li, Y. Zhang, A. Wook, A. Yu, Z. Chen, Energy Environ. Sci. 9 (2016) 2533.
[30] X. Liang, C. Hart, Q. Pang, A. Garsuch, T. Weiss, L.F. Nazar, Nat. Commun. 6 (2015) 5682.
[31] Z. Li, J. Zhang, X.W.D. Lou, Angew. Chem. Int. Ed. 54 (2015) 12886.
[32] J. Zhang, J. Xiang, Z. Dong, Y. Liu, Y. Wu, C. Xu, G. Du, Electrochim. Acta 116 (2014) 146.
[33] X. Tao, X. Chen, Y. Xia, H. Huang, Y. Gan, R. Wu, F. Chen, J. Mater. Chem. A 1 (2013) 3295.
[34] D.P. Hashim, N.T. Narayanan, J.M. Romo-Herrera, D.A. Cullen, M.G. Hahm, P. Lezzi, J.R. Suttle, D. Kelkhoff, E. Muñoz-Sandoval, S. Ganguli, A.K. Roy, D.J. Smith, R. Vajtai, B.G. Sumpter, V. Meunier, H. Terrones, M. Terrones, P.A. Ajayan, Sci. Rep. 2 (2012) 363.
[35] N. Sobczak, J. Schmidt, A. Kazakov, Polish Patent Office, Patent PL166953, 1995.
[36] I. Kaban, R. Nowak, G. Bruzda, L. Xi, N. Sobczak, J. Eckert, L. Giebeler, Carbon 98 (2016) 702.
[37] M.S. Dresselhaus, G. Dresselhaus, A. Jorio, J. Phys. Chem. C 111 (2007) 17887.
[38] H.M. Heise, R. Kuckuk, A.K. Ojha, A. Srivastava, V. Srivastava, B.P. Asthana, J. Raman Spectrosc. 40 (2009) 344.
[39] L. Ma, H.L. Zhuang, S. Wei, K.E. Hendrickson, M.S. Kim, G. Cohn, R.G. Hennig, L.A. Archer, ACS Nano 10 (2016) 1050.
[40] A. Schlange, A.R. dos Santos, U. Kunz, T. Turek, Beilstein J. Org. Chem. 7 (2011) 1412.
[41] B. Zhang, X. Qin, G.R. Li, X.P. Gao, Energy Environ. Sci. 3 (2010) 1531.
[42] J.L. Wang, J. Yang, J.Y. Xie, N.X. Xu, Y. Li, Electrochem. Commun. 4 (2002) 499.
[43] M. Hagen, S. Dörfler, P. Fanz, T. Berger, R. Speck, J. Tübke, H. Althues, M.J. Hoffmann, C. Scherr, S. Kaskel, J. Power Sources 224 (2013) 260.
[44] Y.Z. Fu, A. Manthiram, J. Phys. Chem. C 116 (2012) 8910.
[45] C. Zu, Y. Fu, A. Manthiram, J. Mater. Chem. A 1 (2013) 10362.
[46] M.V. Reddy, T. Yu, C.H. Sow, Z.X. Shen, C.T. Lim, G.V. Subba Rao, B.V.R. Chowdari, Adv. Funct. Mater. 17 (2007) 2792.
[47] J. Balach, H.K. Singh, S. Gomoll, T. Jaumann, M. Klose, S. Oswald, M. Richter, J. Eckert, L. Giebeler, ACS Appl. Mater. Interfaces 8 (2016) 14586.
[48] G. Zhou, L. Li, C. Ma, S. Wang, Y. Shi, N. Koratkar, W. Ren, F. Li, H.-M. Cheng, Nano Energy 11 (2015) 356.
[49] C.P. Yang, Y.X. Yin, H. Ye, K.C. Jiang, J. Zhang, Y.G. Guo, ACS Appl. Mater. Interfaces. 6 (2014) 8789.
[50] M. Hagen, E. Quiroga-González, S. Dörfler, G. Fahrer, J. Tübke, M.J. Hoffmann, H. Althues, R. Speck, M. Krampfert, S. Kaskel, H. Föll, J. Power Sources 248 (2014) 1058.
[51] M. Hagen, P. Fanz, J. Tübke, J. Power Sources 264 (2014) 30.
[52] S. Thieme, J. Brückner, A. Meier, I. Bauer, K. Gruber, J. Kaspar, A. Helmer, H. Althues, M. Schmuck, S. Kaskel, J. Mater. Chem. A 3 (2015) 3808.
[53] E. Peled, F. Patolsky, D. Golodnitsky, K. Freedman, G. Davidi, D. Schneier, Nano Lett. 15 (2015) 3907.
[54] J. Brückner, S. Thieme, H.T. Grossmann, S. Dörfler, H. Althues, S. Kaskel, J. Power Sources 268 (2014) 82.
[55] A. Krause, S. Dörfler, M. Piwko, F.M. Wisser, T. Jaumann, E. Ahrens, L. Giebeler, H. Althues, S. Schädlich, J. Grothe, A. Jeffery, M. Grube, J. Brückner, J. Martin, J. Eckert, S. Kaskel, T. Mikolajick, W.M. Weber, Sci. Rep. 6 (2016) 27982.
[56] M. Hagen, G. Feisthammel, P. Fanz, H.T. Grossmann, S. Dörfler, J. Tübke, M.J. Hoffmann, D. Börner, M. Joos, H. Althues, S. Kaskel, J. Electrochem. Soc. 160 (2013) A996.
[57] Y. Han, X. Duan, Y. Li, L. Huang, D. Zhu, Y. Chen, Mater. Res. Bull. 68 (2015) 160.
[58] Z. Yuan, H.J. Peng, J.Q. Huang, X.Y. Liu, D.W. Wang, X.B. Cheng, Q. Zhang, Adv. Funct. Mater. 24 (2014) 6105.
[59] Y. Fu, Y.S. Su, A. Manthiram, Angew. Chem. 125 (2013) 7068.
[60] H.J. Peng, W.T. Xu, L. Zhu, D.W. Wang, J.Q. Huang, X.B. Cheng, Z. Yuan, F. Wei, Q. Zhang, Adv. Funct. Mater. 26 (2016) 6351.
[61] K. Jin, X. Zhou, L. Zhang, X. Xin, G. Wang, Z. Liu, J. Phys. Chem. C 117 (2013) 21112.
[62] D. Aurbach, E. Pollak, R. Elazari, G. Salitra, C.S. Kelley, J. Affinito, J. Electrochem. Soc. 156 (2009) A694.
[63] G. Zhou, E. Park, G.S. Hwang, A. Manthiram, Nat. Commun. 6 (2015) 7760.
[64] W. Ahn, M.H. Seo, Y.-S. Jun, D.U. Kee, F.M. Hassan, X. Wang, A. Yu, Z. Chen, ACS Appl. Mater. Interfaces 8 (2016) 1984.
[65] Z. Cao, J. Zhang, Y. Ding, Y. Li, M. Shi, H. Yue, Y. Qiao, Y. Yin, S. Yang, J. Mater. Chem. A 4 (2016) 8636.
[66] W.-C. Du, Y.-X. Yin, X.-X. Zeng, J.-L. Shi, S.-F. Zhang, L.-J. Wan, Y.-G. Guo, ACS Appl. Mater. Interfaces 8 (2016) 3584.